# Experimental assessment of a pre-turbo aftertreatment configuration in a single stage turbocharged Diesel engine. Part 2: Transient operation

José Manuel Luján, José Ramón Serrano, Pedro Piqueras *, Óscar García-Afonso

*Universitat Politècnica de València, CMT-Motores Térmicos, Camino de Vera s/n, 46022 Valencia, Spain.*

**Abstract**

This paper corresponds to the second part of a work devoted to analyse the impact of the pre-turbo aftertreatment configuration on the performance of a single stage turbocharged Diesel engine. This second part focuses on the analysis of the engine response under transient operating conditions. To address the causes and effects of the change in engine response several types of transient processes consisting of driving cycles and load transient tests have been evaluated as starting point of the analysis.

These tests make possible to account for the influence of the aftertreatment thermal inertia and how it affects the engine and aftertreatment performance obtained during driving cycles and under highly demanding transient operation. The pre-turbo aftertreatment placement also provides advantages in terms of faster aftertreatment warm-up. Therefore, the benefits on DPF passive regeneration as well as DOC light-off leading to lower gas emissions have been assessed. The results have been compared against baseline emissions measured during experiments with post-turbo aftertreatment placement. Finally the influence of the thermal inertia on driveability in sudden accelerations as a function of the wall temperature along the exhaust line and boosting architecture is assessed combining the analysis of experimental and modelled data.

*Keywords:* Diesel engine, aftertreatment, pre-turbo aftertreatment configuration, transient operation, fuel consumption, emissions

## 1. Introduction

The response of turbocharged Diesel engines under transient operation is a topic of maximum interest for manufacturers and researchers because of its relation with real driving conditions, which are usually falling into the off-design range [1], with important influence on performance and pollutant emissions [2].

The automotive industry is conducting important efforts to the research of the engine transient operation by considering different types of transient patterns, whose main intention is to reproduce properly the real operating conditions of the engine. Driving cycles are the basis for the assessment of the influence on engine performance and pollutant

*P. Piqueras. CMT-Motores Térmicos, Universitat Politècnica de València, Camino de Vera s/n, 46022 Valencia, Spain.
Phone: +34 963877650 Fax: +34 963877659 e-mail: pedpicab@mot.upv.es

emissions of the combustion process [3], fuel characteristics [4], engine mapping [5], etc. Current efforts are driven to the definition of methodologies, based on microtrips [6] and data-driven approaches [7], to update type-approval driving cycles, like the New European Driving Cycle (NEDC), in order to account for more real driving dynamics. Sudden accelerations and decelerations associated to aggressive driving patterns are usual and have become design objective of future cycles. It is the case of the World-Harmonized Light-Duty Vehicles Test Procedure (WLTP) or Real Driving Emissions (RDE) tests [8]. Load transient tests at constant engine speed constitute a type of test involving highly demanding conditions in terms of turbocharger response [9]. As driving cycles, the analysis of load transient processes at constant engine speed is key in the manufacturing and research activity. The focus is put on noise [10] and pollutants [11] generation including fuel blends influence [12], methodologies for combustion characterisation from experimental [13] and modelling [14] approaches and the influence of engine mapping-control for pollutant standards compliance [15]. The turbocharger lag also results critical in tip-in processes with effects on engine driveability [16] and on the peak value of pollutant emissions [17].

Under steady-state operating conditions, modelling [18] and experimental [19] studies regarding pre-turbo aftertreatment configurations have proved that the engine performance is positively affected by the reduction in aftertreatment pressure drop. This pressure drop reduction and its new location gives rise to lower dependence of control parameters on DPF soot loading [20] in contrast with post-turbo aftertreatment placement [21]. However the heat losses taking place across the aftertreatment elements affect negatively. The pulse amplitude reduction across the aftertreatment system is also an additional phenomenon that reduces the instantaneous power at the turbine inlet. Nevertheless, it may benefit from an optimum turbocharger matching in terms of turbine efficiency [22].

Under transient operating conditions, it is necessary to account for the thermal inertia of the aftertreatment substrate on the turbocharger response. The first studies concerning the influence of pre-turbo aftertreament placements under transient operation were carried out during the 80s. An important delay during accelerations from steady-state idle conditions was found [23]. The need to reduce the thermal inertia led to approach low volumes of knitted fibers obtaining a satisfactory engine response at the expense of reducing the filtration efficiency [24].

Recently, several modelling studies with pre-turbo aftertreatment location have confirmed a reduction in turbocharger lag due to the thermal aftertreatment inertia when the engine is subjected to highly dynamic processes being previous conditions of medium-high load [18]. The substrate acts as a energy source heating the cold exhaust gases which come from the cylinders during the low load phase so that the turbocharger speed reduction is avoided and the turbocharger lag disappears in the subsequent acceleration. Nevertheless, there is a the noticeable delay in the turbocharger response with pre-turbo aftertreatment configurations under cold wall operation in single stage turbocharged engines [25]. It has driven to approach for the combined use of this kind of solutions with two stage turbocharging architectures. Bermúdez *et al.* [16] performed a study with a two stage turbocharged HD Diesel engine obtaining successful results in engine driveability by properly managing the boost and EGR valve control during the transient process.

The aim of this work is to cover the lack of experimental data and analysis on the transient response of turbocharged Diesel engines with pre-turbo aftertreatment configuration. The engine response is analysed during the NEDC and load transient tests at constant engine speed. The results of the pre-turbo aftertreatment configuration are compared to that obtained with the traditional post-turbo aftertreatment placement. The influence of the engine thermal conditions is also considered by imposing different initial conditions to every test. On the one hand, it allows evaluating the benefits on aftertreatment warm-up that the pre-turbo aftertreatment placement provides in terms of DPF passive regeneration and DOC light-off during the NEDC. On the other hand, it provides a complete framework to assess the effects of the aftertreatment thermal inertia. In the last part of the paper, a gas dynamic modelling of the engine response under load transient operation at constant engine speed is performed considering the inclusion of a mechanical compressor as a part of the boosting system. A comparison against the experimental data obtained with the single stage turbocharging architecture is performed with both pre-turbo and post-turbo aftertreatment system locations.

## 2. Experimental setup

The study under transient operation has been performed with the same engine and test cell facility that in Part 1 of the work, which is devoted to steady-state operating conditions [19]. Table 1 summarises the main characteristics of the engine in which the tests have been carried out. It is a single stage turbocharged Diesel engine for passenger car applications fulfilling emission standards Euro 4.

Figure 1 shows a scheme of the experimental setup and instrumentation used in the test campaign. The scheme is referred to the engine configuration with post-turbo aftertreatment placement. The setup for the pre-turbo aftertreatment configurations is according to the variations shown in Figure 2. The engine has been installed in a test cell equipped with an asynchronous dynamometer able to control engine speed and torque under steady-state and transient operating conditions. As represented in Figure 1 in grey colour, the engine cooling system and the charge air cooler are connected to external water circuits for temperature control. The main magnitudes defining the engine and aftertreatment performance are measured and ECU variables acquisition is also performed. The location of the thermocouples and pressure sensors along the air path is indicated in Figure 1. The air mass flow has been measured with a hot-wire anemometer and the fuel mass flow by means of a gravimetric balance. Because of the dynamics for transient test measurement the volumetric fuel mass flow provided by the ECU, which is a signal of higher frequency, has been also considered. Nevertheless, since it is not a direct measurement but a calculation, it was calibrated under steady-state operation with the measurements performed by the gravimetric balance according to the methodology proposed by Serrano et al. [13]. For the sake of brevity the reader is referred to Part 1 of the work [19] where further details on the main characteristics of the instrumentation are provided.

The continuous measurement during NEDC tests of the tailpipe exhaust gas emissions downstream of the aftertreatment system has been performed with a Horiba Mexa 7100 DEGR, which provides ±0.5% FSO repeatability

for regulated gaseous emissions. The smoke opacity has been also measured during NEDCs tests with AVL 439 opacimeter. The soot mass is calculated from the measurement of the soot opacity [26]. As indicated in the Part 1 of this work [19] the procedure is considered suitable for comparison proposals since although the application of empirical correlations non-based on mass evaluation can be a source of uncertainty the tests are the same in all the aftertreatment configurations.

As under steady-state operating conditions, the test campaign has covered the assessment of three architectures of the exhaust line differentiated by the aftertreatment placement. Figure 2 shows the three configurations schematically. Plot (a) corresponds to the post-turbo aftertreatment configuration and plots (b) and (c) refer to pre-turbo aftertreatment location in which the relative placement of the DOC and DPF is modified. The objective is to evaluate its influence on engine and aftertreatment performance because of the structural interest of a pre-turbo DPF and metallic DOC placement as a way to protect the turbine blades from the eventual impact of ceramic fragments [27].

### *2.1. Methodology*

In order to provide a representative figure of the engine performance with pre-turbo aftertreatment placement under transient operating conditions, two kind of tests demanding different engine dynamics have been chosen: NEDC and load transient tests at constant engine speed.

The NEDC is a driving cycle that is supposed to represent the typical use of the vehicle in Europe and is applied to evaluate emissions and fuel consumption in passenger cars. It consists of four consecutive urban driving cycles (UDC) followed by a final extra-urban driving cycle (EUDC). Regardless of the ability of the NEDC to represent real driving conditions [28], it has been selected in the present work as a well-known baseline from which assessing the effects on engine performance, regulated emissions and DPF passive regeneration that the placement of the aftertreatment upstream of the turbine brings.

As first step, a single NEDC test has been performed for every exhaust line configuration in order to assess the engine response in terms of performance and emissions. Besides single NEDC, a test consisting of 25 consecutive NEDCs has been carried out due to the fact that the raw particulate matter emission during one NEDC is very low and introduces high uncertainty in the evaluation of the regenerated soot mass. In this case, the post-turbo aftertreatment configuration and the pre-turbo DOC and DPF configuration have been compared. Additionally it provides reliable conditions for a confident evaluation of the fuel economy. The test was performed according to the following steps:

1. Before the beginning of the test, the DPF was regenerated. Afterwards, the clean DPF was immediately weighed in hot conditions.
2. The first part of the whole test, which consisted of 16 consecutive NEDCs, was performed. The first NEDC was tested in cold conditions. When the testing of the NEDCs ended up, the DPF was weighed in hot conditions to obtain the soot mass remaining in the substrate.
3. The whole test was completed performing 9 additional NEDCs beginning again from cold starting conditions. Finally, the DPF was weighed at the end of the test to quantify the total amount of soot accumulated in the DPF.

Since the NEDC is a driving cycle of low dynamics, the assessment of the engine response with the pre-turbo aftertreatment configuration is completed with a load transient test at constant engine speed. This process is useful to evaluate the effect of the aftertreatment thermal inertia on the engine driveability. The pedal demand, i.e. the input variable of the ECU related to the throttle position, is represented in Figure 3. The test comprised the following phases:

1. The engine ran at steady-state under motoring conditions (no injected fuel mass, pedal at 0%) at 2000 rpm.
2. The pedal was pushed up from motoring conditions to 80% in engine load in 0.2 s keeping constant the engine speed. This phase is referred as cold wall operation since wall temperature remains low during the load step due to thermal inertia.
3. The engine was stabilised at 80% of load and 2000 rpm during 600 s.
4. The pedal was drop down from 80% in engine load up to motoring conditions in 0.2 s keeping constant the engine speed.
5. After 5 s at motoring conditions, the pedal was again pushed up to 80% in engine load in 0.2 s. This phase is referred as hot wall operation since wall temperature remains high during the load step due to thermal inertia.

## 3. Results and discussion

### *3.1. New European Driving Cycle*

Figure 4 shows in plot (a) the accumulated fuel consumption along the test of a single NEDC for each aftertreatment system configuration considered in the study. In order to show the repeatability of the tests, results corresponding to cycle 1 of the consecutive 25 NEDCs tested with post-turbo and pre-turbo DOC&DPF configurations are included. Both pre-turbo aftertreatment configurations are able to overcome the UDC conditions and most of the EUDC without relevant damage on the fuel consumption in comparison with the post-turbo aftertreatment configuration. This result is in good agreement with the experimental results obtained under steady-state operating conditions in points selected from the NEDC and described in the Part 1 of the work [19]. Under steady-state operating conditions at low engine load and speed, the reduction in aftertreatment pressure drop and the fact that it is not multiplied by the pressure ratio to set the engine back-pressure are not completely able to compensate the pulse amplitude reduction across the aftertreatment system in pre-turbo placement. As a consequence a slight damage in fuel consumption is obtained. It is also observed in the accumulated fuel consumption along the NEDC shown Figure 4(a).

However, the last acceleration of the EUDC, at time 1150 s, is clearly demanding more fuel injection to pre-turbo aftertreatment configurations to reach the vehicle speed requirements. It causes a fuel penalty in both pre-turbo configurations. Considering the mean accumulated fuel consumption of the two NEDC tests represented for the post-turbo aftertreatment configuration, the fuel penalty ranges between 4% and 8%, which are the values for pre-turbo DPF and DOC placement and pre-turbo DOC and DPF placement respectively.

The reason of the penalty in fuel consumption affecting pre-turbo aftertreatment placement is related to the thermal inertia of the aftertreatment elements. It inhibits the turbine inlet temperature increase in sudden accelerations and hence results in the lack of energy for the expansion process. As a consequence, the VGT position is closer in pre-turbo aftertreatment configurations than in the case of the post-turbo aftertreatment configuration during all the EUDC, as shown in Figure 4(b). As average value, the VGT position increases its value in a 15% in the pre-turbo aftertreatment configurations with respect to the post-turbo aftertreatment configuration from time 825 s s to 1150 s.

It is not very damaging in terms of fuel consumption in most of the EUDC since pre-turbo aftertreatment placement benefits from the aftertreatment pressure drop location [19]. However, the last acceleration is requiring not only further VGT closing but also higher pedal demand, which is plotted in Figure 4(c), and hence higher fuel consumption during this phase.

Nevertheless, it is important to note that this study has not included a control optimization of the pre-turbo aftertreatment configuration. The analysis of the VGT closing in Figure 4(b) indicates that it may have been further closed contributing to engine acceleration without the need of additional pedal demand. It probably would have led to lower or even null fuel penalty, similarly to the first part of the EUDC. In fact, VGT opens during the last acceleration with pre-turbo aftertreatment placement, following the same strategy as the post-turbo aftertreatment location. This discussion is strengthened by the fact that current pedal strategy is leading during last acceleration to unnecessary equivalence ratios over stoichiometric conditions, as forward shown in Section 3.1.1.

The analysis of the temperature profile in different locations of the exhaust line also underlines the convenience of pedal limitation. The evolution of the gas temperature along the exhaust line is shown in Figure 5. In this case, results for cycle 1 of the consecutive NEDC testing are also shown and verify that temperature variations between tests with the same exhaust configuration are negligible. Plot (a) represents the gas temperature at the VGT inlet. In post-turbo aftertreatment placement this temperature is completely related to the engine dynamics despite the exhaust manifold thermal inertia. However, cold wall conditions are making that the VGT inlet temperature is completely governed by the aftertreatment thermal inertia and drifted with respect to the engine dynamics in the case of any of the proposed pre-turbo aftertreatment configurations. As a consequence, the lack of thermal energy at the turbine inlet requires the previously indicated greater VGT closing. With respect to the last acceleration during the EUDC, it can be seen that the increase of pedal during this phase in pre-turbo aftertreatment configuration contributes to increase the VGT inlet temperature. However such an increase reaches only 20 $^{o}$C during the time is lasting the acceleration of the vehicle being most of the increase delayed by the aftertreatment thermal inertia. Because of the temperature drift, the fuel penalty may have been reduced by acting on the VGT closing and limiting the maximum equivalence ratio.

Figure 5 represents the DPF and DOC inlet temperature in plots (b) and (c) respectively as a function of the aftertreatment placement. As expected, the pre-turbo aftertreatment configurations ensure an increase of the temperature level across the aftertreatment elements with respect to that taking place in post-turbo placement. In order of magnitude, the temperature increase is around 70 $^{o}$C during UDC phases and higher than 200 $^{o}$C during the final EUDC phase. This fact involves better conditions for faster DOC light-off and soot oxidation due to passive regeneration.

It is also interesting to note that the VGT inlet temperature is affected by the relative DOC and DPF placement in pre-turbo configuration being lower in the case of prior DOC location. It is especially relevant during the EUDC and leads to higher fuel penalty in this configuration. The cause lies in the placement of the substrate with higher thermal inertia, i.e. DPF, in the last position. When the DPF is placed next to the exhaust manifold, its inlet temperature is maximum and directly related to the engine operation. It speeds up the DPF heating. Although this process involves an initial damage of the DOC thermal transient, finally the whole system gets a faster thermal response. Similar results would be obtained regarding the analysis of different aftertreatment solutions such as LNT and DPF or FSCR combinations.

Considering the different aftertreatment solutions for pollutant emissions abatement currently available, it is interesting to analyse the VGT outlet temperature because of the possibility to combine pre-turbo and post-turbo aftertreatment configurations. Figure 5(d) shows the gas temperature profile during the NEDC at the outlet of the last element in each configuration, which has been referred as exhaust line temperature. Therefore, it corresponds to the gas temperature at DPF outlet in the case of the post-turbo aftertreatment configuration. In the same way, the term exhaust line temperature denotes the gas temperature at VGT outlet in the case of the pre-turbo aftertreatment configuration. In both aftertreatment configurations it would coincide with the gas temperature at the inlet of an SCR system if it were installed in the exhaust line (not present in the current study). Although the SCR catalyst provides low conversion efficiency up to 210 $^{o}$C [29], below 180$^{o}$C the ammonia can react with $NO_2$ producing undesired $NH_4NO_3$ [30]. Therefore, the dosing of urea is not performed below this temperature. In this context, the pre-turbo configuration would provide higher temperature (30 – 50 $^{o}$C) at the inlet of the SCR in comparison with the post-turbo configuration from the second UDC, what would contribute to reduce the heat-up strategies [31] and to increase the $NO_x$ conversion efficiency at the end of the cycle.

Change in temperature level across the aftertreatment elements is directly affecting exhaust gaseous emissions. Figure 6 depicts the accumulated emission of regulated pollutants during the NEDC as a function of the aftertreatment placement. Plots (a) and (b) are devoted to CO and HC tailpipe emissions, i.e. related to the DOC light-off and conversion efficiency. The location of the light-off is repetitive in tests with the same aftertreatment configuration despite of slight differences in the accumulated emission for CO and HC. The results clearly certify the faster DOC light-off both for CO and HC emissions in pre-turbo aftertreatment configurations. The earliest light-off is obtained in the case of DOC and DPF relative placement. The rate of CO emission increase becomes close to zero about 500 s after the NEDC beginning with pre-turbo DOC and DPF placement and about 550 s in the case of pre-turbo DPF and DOC placement. It means an advance in maximum conversion efficiency with respect to the post-turbo aftertreatment placement ranging between 295 s and 345 s as a function of the relative DOC and DPF in pre-turbo configuration. The result is a reduction in CO emission higher than 14% with the underfloor DOC placed upstream of the VGT and without close-coupled DOC. It highlights the potential for faster DOC light-off and volume reduction [32]. Similar results are obtained with respect to HC emission, which is shown in Figure 6(b). HC emission undergoes

a reduction in the tailpipe ranging between 8% and 15% with respect to post-turbo DOC placement depending on the DOC placement in pre-turbo configuration.

$NO_x$ and particulate matter accumulated emissions along the NEDC are represented in Figure 6(c) and (d) respectively. The trend in the accumulated emission is in agreement with results obtained under steady-state operating conditions [19]. Both $NO_x$ and particulate matter emissions are slightly lower with pre-turbo aftertreatment placement up to the last acceleration of the EUDC. From it there is higher raw $NO_x$ and particulate matter emissions because of the higher pedal demand which in turn causes higher tailpipe emissions, as plots (c) and (d) in Figure 6 evidence. Nevertheless, the differences are not remarkable regarding pollutant standards fulfilment and would be still subjected to the engine control optimization during the EUDC.

*3.1.1. Consecutive NEDCs testing*

As additional test, the measurement of 25 consecutive NEDCs was performed according to the methodology described in Section 2.1. One of the objectives is to evaluate with higher accuracy the effect of the global fuel consumption of the pre-turbo aftertreatment configuration under driving conditions. The pre-turbo DOC&DPF configuration was selected since it showed to be the most damaging architecture in terms of fuel economy during a NEDC starting from cold conditions. Figure 7 shows the evolution of the accumulated fuel consumption along the 25 NEDCs. The total fuel consumption corresponding to the post-turbo aftertreatment placement is 10.83 kg. In the case of the pre-turbo DOC&DPF configuration the fuel consumption raises up to 11.16 kg, what means a fuel penalty of 3%. It involves a reduction in fuel penalty from 8% to 3% when the pre-turbo aftertreatment effect is compared between an only cold NEDC and a driving sequence of 25 NEDCS including an intermediate stop. The previously indicated potential optimization of the VGT and pedal control to avoid abnormally high equivalence ratio has not been considered in any case. Additionally, and according to the results from the cold NEDC, the fuel consumption may be improved by the relative DPF&DOC placement in pre-turbo configuration.

The fuel penalty obtained in the 25 consecutive NEDCs test is explained by the difference in temperature profile at the VGT inlet during cold and hot cycles. Cold cycle temperature profiles have been previously shown in Figure 5, whereas Figure 8 shows them at VGT, DPF and DOC inlet for hot cycles 12 and 25. No differences are found in temperature measurement between hot cycles what again confirms repeatability. Figure 8(a) shows that the VGT inlet temperature during the last 200 s of the hot NEDCs is slightly higher ($\sim 25\,^{o}C$) than that obtained in the cold NEDC. It still causes fuel penalty with respect to the post-turbo aftertreatment placement during this phase of the cycle. Nevertheless this fuel penalty gets reduced since the requirements on pedal control are less severe. As shown in Figure 9, during the last acceleration of the EUDC the engine control imposes a pedal requirement that leads to a peak of equivalence ratio equal to 1.4 in the cold NEDC with pre-turbo DOC&DPF configuration. It causes the unnecessary increase of the fuel consumption and soot emission. The peak of equivalence ratio is reduced to stoichiometric conditions in the case of hot NEDCs but it is still higher than the value of the cold NEDC with post-turbo aftertreatment configuration. This behaviour is offset during the first two UDCs in which the temperature profile

at the VGT inlet is clearly over the obtained with post-turbo aftertreatment (Figure 8(a)) because of the aftertreatment thermal inertia. The monolith substrate contributes to heat the exhaust gas flow. Consequently there is a slight improvement of the fuel consumption during this driving phase and hence it is obtained a cycle to cycle compensation of the fuel damage produced at the end of the NEDC.

Plots (b) and (c) in Figure 8 represent the temperature at the DPF and DOC inlet respectively during a hot NEDC. There is a high temperature level during the first two UDCs regardless the aftertreatment placement. The temperature converges at the EUDC beginning to the magnitude that is also obtained in a cold NEDC. For the case of the DOC, the thermal level reached is high enough to ensure good conversion efficiency independently of the DOC placement. This can be also extrapolated to pre-turbo DPF&DOC placement. Nevertheless, the difference in temperature level between pre- and post-turbo placement is clearly favouring the passive soot regeneration in the first case. Figure 10 represents the accumulated filtrated soot mass in the DPF during the 25 NEDCs test for both pre- and post-turbo aftertreatment configurations. As previously indicated, it has been calculated from opacity measurements by means of the correlation proposed by Bermúdez *et al.* [26]. The mass of filtrated soot is approximately 20% higher in the case of the pre-turbo aftertreatment placement. It is due to the particulate matter emission increase caused by equivalence ratio over 1 to which the pedal and boost control is leading during the last acceleration of the EUDC in every NEDC.

Additionally, the DPF was weighed at the end of cycles 16 and 25. On the one hand, comparing filtrated and weighed soot mass it is possible to conclude that lack of passive regeneration is obtained in the case of post-turbo DPF placement. The estimate of filtrated soot mass in cycles 16 and 25 almost coincides with the corresponding weighing result for this configuration. In fact, the estimated filtrated soot mass is lower than the weighed value being the most probably cause of this result the uncertainty of the opacity to soot mass correlation used in this work. Despite the accuracy of used correlation is not perfect, it has been considered enough for the demonstrative and comparative purposes of this work.

On the other hand, the weighed soot mass is almost 25% lower than the filtrated mass in the case of the pre-turbo aftertreatment configuration. This great difference confirms, in agreement with the results obtained under steady-state operation shown in the Part 1 of the work [19], the capability of this pre-turbo exhaust line architecture to promote passive regeneration.

### *3.2. Load transient test at constant engine speed*

#### *3.2.1. Cold wall operation*

The thermal inertia of the aftertreatment system has been already shown to be the main concern of pre-turbo aftertreatment placement on engine driveability. It drives the interest to load transient tests at constant engine speed as a key test to assess the engine dynamic response. Figure 11 shows the engine performance as a function of the aftertreatment placement in a load transient test under cold wall operation in which the engine is driven from motoring conditions to 80% in engine load at 2000 rpm.

Under these operating conditions, the torque evolution, which is plotted in Figure 11(a), clearly indicates the dramatic influence of the pre-turbo aftertreatment placement on the engine driveability with a single stage turbocharging architecture. The initial torque response only covers 70% of the torque provided by the post-turbo aftertreatment placement. Instantaneously, the pre-turbo aftertreatment placement is imposing a reduced torque step governed by the initial lack of turbocharger response. There is not effect on the air mass flow, shown in Figure 11(b), being the injected fuel mass (Figure 11(c)) limited by the boost control. It further affects negatively the turbocharger lag and leads to a snowball effect. The target in injected fuel mass is reached 101.7 s after the beginning of the load transient test in the case of the pre-turbo DPF and DOC placement, and 106.2 s when a pre-turbo DOC and DPF placement is adopted.

Figure 12 shows in plot (a) that there is not change in turbocharger speed at the beginning of the transient with pre-turbo aftertreatment placement. Since the engine is driven from motoring conditions it involves to operate like an naturally aspirated engine without the possibility to take advantage of the single stage boosting system, as the boost pressure profile evidences in Figure 12(b).

The engine dynamics is being fully controlled by the thermal inertia of the aftertreatment monoliths. Plots in Figure 13 represent the temperature along the exhaust line. The DPF and DOC thermal inertia, whose temperature profiles are represented in plots (a) and (b) respectively, prevents the gas temperature from increasing at the inlet of the VGT with a pre-turbo aftertreatment placement, as shown in Figure 13(c). Although the engine response is not acceptable in terms of driveability, it is interesting to note that the DPF and DOC relative placement slightly accelerates the thermal transient. In agreement with the discussion in Section 3.1, the DPF monolith mass is governing the thermal transient. The previous placement of the DOC imposes a reduction in the DPF inlet temperature, what consequently increases the thermal transient duration. This process is reverted by placing the DPF just at the outlet of the exhaust manifold. Initially it damages the DOC thermal transient but finally improves the rate of temperature increase both at the DOC and VGT inlets and leads to a faster thermal transient.

Although the aftertreatment is imposing a lag on the available power at the VGT inlet, the ability of the boosting system to recover the engine driveability is also closely related to its architecture. To address this topic, the engine response with pre-turbo aftertreatment system and the assistance of a mechanical compressor has been modelled with OpenWAM$^{TM}$[33]. The corresponding engine architecture is sketched in Figure 14. OpenWAM $^{TM}$ is an open-source gas dynamics code developed at CMT-Motores Térmicos used for internal combustion engine modelling [34]. The model solves the governing equations for one-dimensional unsteady compressible non-homentropic flow. The flow properties are transported along 1D elements solved by means of shock capturing methods, 0D elements solved by means of filling-and emptying models and boundary conditions solved by the method of characteristics. The combination of these kinds of elements allows modelling the behaviour of the different engine components. This is observed in the engine scheme of the OpenWAM's interface corresponding to the pre-turbo DPF&DOC configuration shown in Figure 15. In this figure, the big rectangles and squares represent 0D elements and the small size squares represent boundary conditions. 1D elements are represented by solid lines connecting boundary conditions.

The main components of the engine are indicated in Figure 15: cylinders, in which the combustion process is modelled as a function of the crank angle and the engine operating conditions using an interpolation methodology on a rate of heat release database [14]; charge air and EGR coolers, which are modelled as pipe beams with inlet and outlet volumes [35]; specific models for compressors [36] and turbines [37]; and aftertreatment systems with focus on fluid dynamic aspects for accurate pressure drop and acoustic prediction [38] besides the influence of the heat transfer effects [39] and the consideration of clean [40] and soot loaded substrate [41] in the case of the DPF.

As first step, the engine test with pre-turbo DPF&DOC configuration was modelled in OpenWAM$^{TM}$. Details on the model validation under steady-state operating conditions can be found in [42], in which an analysis of DPF sizing in post-turbo and pre-turbo placement is performed. The modelling under transient operation is presented in Figures 16- 18. In these figures the dashed red line represents the model results obtained with the single stage turbocharging architecture, which are compared with the experimental data. It can be observed that the model is able to predict properly the main aspects that describe the engine transient response with this architecture: engine performance (Figure 16), turbocharger dynamics (Figure 17) and aftertreatment thermal inertia (Figure 18). The good reproduction of these aspects results in a reliable starting point for the prediction of the engine response with a two stage boosting architecture based on the inclusion of a mechanical compressor. The modelled engine performance when a mechanical compressor assisting the turbocharger is incorporated is represented in Figure 16 in green colour. With the proposed boosting system the target torque is reached instantaneously, as represented in Figure 16(a), recovering the engine driveability. It is due to the fact that the mechanical compressor is providing a sudden increase of the boost pressure up to the target value, which leads to the instantaneous increase of the air mass flow (Figure 16(b)) and hence to the injection of the target fuel mass without any delay imposed by the smoke limiter (Figure 16(c)).

Figure 17 focuses on the behaviour of the turbocharging system. Plot (a) in Figure 17 shows that the turbocharger speed stabilises at a lower level when the mechanical assistance for boosting is applied. The control of the VGT closing to divide the pressure ratio between the turbocompressor and the mechanical compressor is allowing to reach such a condition. Plot (b) represents the power supply to the mechanical compressor, which has a peak of 3 kW. It gives as a result a transient fuel consumption damage. As the thermal transient of the aftertreatment elements is overcome the power supplied to the mechanical compressor reduces below 2.5 kW. This setting enables controlling the VGT opening to avoid the bsfc damage with respect to the post-turbo aftertreatment placement for this operating point before the thermal transient end, as Figure 17(c) shows.

A benefit for the pre-turbo aftertreament configuration appears in terms of increase of VGT inlet temperature due to the fact that the maximum injected fuel mass and air mass flow are reached from the very beginning of the transient phase. Figure 18(a) shows that the DPF inlet temperature when the mechanical compressor is included is approximately the same as that obtained with the single stage turbocharging architecture, despite of the differences in fuel and mass flow (the same maximum equivalence ratio is kept). The increase of the mass flow across the DPF monolith keeping constant gas temperature reduces the heat transfer due to the lower dwell time [39] and leads to a higher rate of temperature increase at the DOC inlet, as represented in Figure 18(b). As a consequence, the VGT

inlet temperature increase is also accelerated. Figure 18(c) shows that it is kept higher during the tip-in process when the mechanical compressor is used. In turn this behaviour improves the conditions for the boosting system control providing greater flexibility. Besides engine boosting, such a flexibility may be driven to the thermal management of the aftertreatment system placed downstream of the VGT by means of the control on the VGT outlet temperature and the change in boosting demand to the mechanical compressor.

*3.2.2. Hot wall operation*

Under cold wall operation the aftertreatment system acts as a sink accumulating thermal energy and conditioning the engine driveability. This characteristic turns positive when the transient process is taking place under hot wall conditions since the ceramic substrate becomes a source of power heating the exhaust mass flow. Figure 19 shows the experimental engine performance during such a test for each aftertreatment configuration. Initially the engine is operating under steady-state condition at 2000 rpm and 80% in engine load. According to Figure 3, the pedal is drop down driving the engine to motoring conditions during 5 s. Then the pedal is finally pushed up again up to 80% in engine torque keeping constant the engine speed.

Figure 19(a) shows that the target torque is reached slightly faster with any of the pre-turbo aftertreatment configurations. The slight delay obtained with post-turbo aftertreatment placement is due to the turbocharger lag. With this configuration the air mass flow goes down when the engine is driven to motoring conditions, as represented in plot (b). However, it does not happen in the configuration with pre-turbo aftertreatment placement, in which the air mass flow suffers only a slight drop and then increases even during the motoring phase. As a consequence, when the pedal is again pushed up, the smoke limiter acts in the case of the post-turbo aftertreatment placement delaying the fuel injection and hence the engine response. Figure 19(c) shows that the injection of the target fuel mass is not affected by the smoke limiter if the pre-turbo aftertreatment configurations are considered.

As previously discussed, the reason for this engine response lies in the energy released by the aftertreatment substrate during the motoring phase. The comparison of the VGT inlet temperature as a function of the aftertreatment placement, which is represented in Figure 20(a), reveals that the pedal drop off causes an important reduction of the VGT inlet temperature in the case of post-turbo aftertreatment placement, even taking into account the thermocouple thermal inertia. This expected behaviour gives as a result the sudden reduction in turbocharger speed and boost pressure, which are represented in Figure 20(b) and 20(c) respectively, and hence the air mass flow decrease.

However, the VGT inlet temperature is not affected by the engine pedal drop off and the subsequent tip-in process with pre-turbo aftertreatment configurations. The ceramic monolith heats the exhaust mass flow during these phases providing constant temperature at the inlet of the VGT. It avoids the reduction of the turbocharger speed as represented in Figure 20(b) and the appearance of any lag in the next torque demanding phase. In the tested case, and taking into account that the original ECU calibration was not modified, there is even an increase of the turbocharger speed. Figure 20(c) evidences that it leads to exceed the target boost pressure at the beginning of the transient what produces an initial VGT opening followed by the subsequent stabilisation.

## 4. Summary and conclusions

This work comprises the second part of an experimental study of pre-turbo aftertreatment placement to analyse the impact of this kind of architecture on a turbocharged Diesel engine for passenger car applications. The analysis has covered the engine operation, performance and emissions and a comparison with the traditional post-turbo aftertreatment configuration. This second part of the work is focused on transient operating conditions.

The analysis of the NEDC driving cycle has shown that the pre-turbo aftertreatment configuration is able to follow the driving conditions imposed by the cycle in spite of the cold start conditions. However, the aftertreatment thermal inertia makes necessary an increase of the VGT closing during the EUDC and an increase of the pedal demand during the last acceleration of this phase, which finally causes a fuel penalty. It ranges around 4% for pre-turbo DPF&DOC configuration and 8% for the case of pre-turbo DOC&DPF configuration. The difference is related to the faster thermal transient taking place when the greater thermal inertia element, i.e. DPF, is located next to the exhaust manifold.

A consequence of the aftertreatment thermal inertia is that the VGT inlet temperature rise does not occur during the last acceleration of the NEDC but it is drifted to the end of the cycle. Therefore, the engine control may be improved by closing further the VGT and avoiding pedal increase leading to equivalence ratios over stoichiometric conditions, such as these found during the engine testing with pre-turbo aftertreatment. Consequently, the fuel penalty would be reduced in cold NEDCs. Nevertheless, the results have found that during 25 consecutive NEDCs with an intermediate stop, the fuel penalty with the most damaging pre-turbo DOC&DPF architecture is reduced from 8% in a cold NEDC to an averaged 3% without any optimization of the pedal strategy, which is to be performed in future works. This result also highlights the importance of the engine application, i.e. the characteristic driving cycle. Driving cycles with frequent accelerations up to high engine load would be benefited in terms of fuel consumption, as it was inferred from results under steady-state operation shown in Part 1 of this work, because of the lower weighed influence of the cold transient operation during the whole cycle.

Concerning engine emissions, the high thermal level in the pre-turbo aftertreatment is leading to faster DOC light-off reducing CO and HC emissions during the NEDC. Reduction is around 15% in pre-turbo DOC&DPF placement and slightly lower if the DOC is placed downstream of the DPF. This reduction has been achieved removing the additional close-coupled DOC used in the post-turbo aftertreatment configuration. It underlines the potential for aftertreatment volume reduction what would provide lower thermal inertia and cost savings. The $NO_x$ emissions are not affected whereas a slight increase in particulate matter emission has been found. It has been caused by the higher raw emission during the EUDC because of the higher VGT closing and pedal demand. Nevertheless the tailpipe soot emission is still lower than that required for the oncoming Euro 6 standards. Additionally the test of 25 consecutive NEDCs has confirmed the ability of the pre-turbo DPF placement to promote passive regeneration because of the higher temperature despite the transient operation. The 24% of the filtrated soot mass has been passively regenerated with a pre-turbo DOC&DPF configuration.

The analysis of experimental results corresponding to load transient tests at constant engine speed are in agreement with modelling predictions shown in previous author's works. On the one hand, hot wall operation benefits from a positive impact of the aftertreatment thermal inertia. The monoliths heat the gases from the exhaust manifold to the VGT inlet during the low load phase. Consequently almost constant turbocharger speed and high boost pressure remain, so that the subsequent tip-in process is not suffering turbocharger lag. However, the thermal inertia of the aftertreatment becomes a critical phenomena under cold wall operation. It constrains the abilitiy of the engine to provide the expected driveability. Modelling analysis performed by means of 1D computational tools has shown that the engine dynamic response can be recovered with a two stage boosting system, although with a penalty in fuel economy during the cold transient phase.

## Acknowledgements

This work has been partially supported by the Spanish Ministry of Economy and Competitiveness through Grant No. TRA2013-40853-R.

## References

[1] Giakoumis EG, Alafouzos AI. Study of Diesel engine performance and emissions during a transient cycle applying an engine mapping-based methodology. Appl Energ 2010;87(4):1358–65.

[2] Fontaras G, Franco V, Dilara P, Martini G, Manfredi U. Development and review of Euro 5 passenger car emission factors based on experimental results over various driving cycles. Sci Total Environ 2014;468-469:1034–42.

[3] Pacheco AF, Martins MES, Zhao H. New European Drive Cycle (NEDC) simulation of a passenger car with a HCCI engine: Emissions and fuel consumption results. Fuel 2013;111:733–9.

[4] Armas O, García-Contreras R, Ramos A. Impact of alternative fuels on performance and pollutant emissions of a light duty engine tested under the New European Driving Cycle. Appl Energ 2013;107:183–90.

[5] Giakoumis EG, Lioutas SC. Diesel-engined vehicle nitric oxide and soot emissions during the european light-duty driving cycle using a transient mapping approach. Transport Res D-Tr E 2010;15(3):134–43.

[6] Xiao Z, Dui-Jia Z, Jun-Min S. A synthesis of methodologies and practices for developing driving cycles. Energy Procedia 2012;16:1868–73.

[7] Bishop JDK, Axon CJ, McCulloch MD. A robust, data-driven methodology for real-world driving cycle development. Transport Res D-Tr E 2012;17(5):389–97.

[8] Karsten R, Grisstede I, Franoschek S, Seyler M, Hoyer R, Noack H, Basso S, Müller W. Diesel NOx-aftertreatment systems for upcoming LDV-emission legislations. In: SAE ATA Convergence Conference, Torino, Italy, 2012.

[9] Payri F, Benajes J, Galindo J, Serrano JR. Modelling of turbocharged Diesel engines in transient operation. Part 2: Wave action models for calculating the operation in a High Speed Direct Injection engine. P I Mech Eng D-J Aut 2002;216:479–93.

[10] Giakoumis EG, Dimaratos AM, Rakopoulos CD. Experimental study of combustion noise radiation during transient turbocharged Diesel engine operation. Energy 2011;36(8):4983–95.

[11] Rakopoulos CD, Dimaratos AM, Giakoumis EG, Rakopoulos DC. Evaluation of the effect of engine, load and turbocharger parameters on transient emissions of Diesel engine. Energ Convers Manage 2009;50(9):2381–93.

[12] Rakopoulos CD, Dimaratos AM, Giakoumis EG, Rakopoulos DC. Investigating the emissions during acceleration of a turbocharged diesel engine operating with bio-diesel or n-butanol diesel fuel blends. Energy 2010;35(12):5173–84.

[13] Serrano JR, Arnau FJ, Dolz V, Piqueras P. Methodology for characterization and simulation of turbocharged Diesel engines combustion during transient operation. Part 1: Data acquisition and post-processing. Appl Therm Eng 2009;29(1):142–9.

[14] Serrano JR, Climent H, Guardiola C, Piqueras P. Methodology for characterisation and simulation of turbocharged Diesel engines combustion during transient operation. Part 2: Phenomenological combustion simulation. Appl Therm Eng 2009;29(1):150–8.

[15] Serrano JR, Arnau FJ, Dolz V, Tiseira A, Lejeune M, Auffret N. Analysis of the capabilities of a two-stage turbocharging system to fulfil the US2007 anti-pollution directive for heavy duty Diesel engines. Int J Automot Techn 2008;9(3):277–88.

[16] Bermúdez V, Serrano JR, Piqueras P, García-Afonso O. Analysis of heavy-duty turbocharged Diesel engine response under cold transient operation with a pre-turbo aftertreatment exhaust manifold configuration. Int J Engine Res 2013;14(4):341–53.

[17] Rakopoulos DC, Dimaratos AM, Giakoumis EG, Rakopoulos CD. Study of turbocharged Diesel engine operation, pollutant emissions and combustion noise radiation during starting with bio-diesel or n-butanol diesel fuel blends. Appl Energ 2011;88:214–24.

[18] Bermúdez V, Serrano JR, Piqueras P, García-Afonso O. Assessment by means of gas dynamic modelling of a pre-turbo diesel particulate filter configuration in a turbocharged HSDI Diesel engine under full-load transient operation. P I Mech Eng D-J Aut 2011;225(9):1134–55.

[19] Luján JM, Bermúdez V, Piqueras P, García-Afonso O. Experimental assessment of pre-turbo aftertreatment configurations in a single stage turbocharged Diesel engine. Part 1: Steady-state operation. Energy, In Press, doi:10.1016/j.energy.2014.05.048, 2014.

[20] Bermúdez V, Serrano JR, Piqueras P, García-Afonso O. Influence of DPF soot loading on engine performance with a pre-turbo aftertreatment exhaust line. In: SAE Technical Paper 2012-01-0362, 2012, doi:10.4271/2012-01-0362.

[21] Lapuerta M, Rodríguez-Fernández J, Oliva F. Effect of soot accumulation in a diesel particle filter on the combustion process and gaseous emissions. Energy 2012;47:543–52.

[22] Payri F, Serrano JR, Piqueras P, García-Afonso O. Performance analysis of a turbocharged heavy duty Diesel engine with a pre-turbo diesel particulate filter configuration. SAE Int J Engines 2011;4(2):2559–72.

[23] Hiereth H. Daimler-Benz AG car test with a free-running pressure-wave charger - A study for an advanced supercharging system. In: SAE Technical Paper 890453, 1989, doi:10.4271/890453.

[24] Jenny E, Hansel J, Mayer A. The transient behavior of supercharged passenger car Diesel engines fitted with particulate traps. In: SAE Technical Paper 890171, 1989, doi:10.4271/890171.

[25] Subramaniam MN, Joergl V, Keller P, Weber O, Toyoshima T, Vogt CD. Feasibility assessment of a pre-turbo after-treatment system with a 1D modeling approach. In: SAE Technical Paper 2009-01-1276, 2009, doi:10.4271/2009-01-1276.

[26] Bermúdez V, Luján JM, Serrano JR, Pla B. Transient particle emission measurement with optical techniques. Meas Sci Technol 2008;19:0654004.

[27] Payri F, Desantes JM, Piqueras P, Serrano JR. Device for treating exhaust gases from Diesel turbo-supercharged reciprocating internal combustion engines (RICE). Patent WO 2013/041747 A1. Priority date 23/09/2011. European Patent Office. (2013).

[28] Mock P, German J, Bandivadekar A, Riemersma I. Discrepancies between type approval and ”real-world fuel consumption and CO2 values. Assessment for 2001-2011 European passenger cars. In: ICCT International Council on Clean Transportation, 2012.

[29] De Rudder K. High efficiency SCR for non-road applications. In: Thermo-and Fluid-Dynamic Processes in Direct Injection Engines 2012, Valencia, Spain, 2012.

[30] Heck RM, Farrauto RJ. Catalytic air pollution control, Commercial Technology, Hoboken, New Jersey: John Wiley & Sons Inc.; 2009.

[31] Tourlonias P, Koltsakis GC. Model-based comparative study of Euro 6 diesel aftertreatment concepts, focusing on fuel consumption. Int J Engine Res 2011;12:238–51.

[32] Serrano JR, Guardiola C, Piqueras P, Angiolini E. Analysis of the aftertreatment sizing for pre-turbo DPF and DOC exhaust line configuration. In: SAE Technical Paper 2014-01-1498, 2014, doi:10.4271/2014-01-1498.

[33] Openwam website, CMT-Motores Térmicos (Universitat Politècnica de València). www.openwam.org (2014).

[34] Galindo J, Serrano JR, Arnau FJ, Piqueras P. Description of a Semi-Independent Time Discretization methodology for a one-dimensional gas dynamics model. J Eng Gas Turb Power 2009;131:034504.

[35] Galindo J, Serrano JR, Arnau FJ, Piqueras P. Description and analysis of a one-dimensional gas-dynamic model with Independent Time Discretization. In: Proceedings of the ASME Internal Combustion Engine Division 2008 Spring Technical Conference ICES2008, 2008.

[36] Torregrosa A, Arnau FJ, Piqueras P, Reyes-Belmonte M. Acoustic one-dimensional compressor model for integration in a gas-dynamic code. In: SAE Technical Paper 2012-01-0834, 2012, doi:10.4271/2012-01-0834.

[37] Payri F, Serrano JR, Fajardo P, Reyes-Belmonte MA, Gozalbo-Belles R. A physically based methodology to extrapolate performance maps of radial turbines. Energ Convers Manage 2012;55:146–63.

[38] Torregrosa AJ, Serrano JR, Arnau FJ, Piqueras P. A fluid dynamic model for unsteady compressible flow in wall-flow diesel particulate filters. Energy 2011;36:671–84.

[39] Galindo J, Serrano JR, Piqueras P, García-Afonso O. Heat transfer modelling in honeycomb wall-flow diesel particulate filters. Energy 2012;43:201–13.

[40] Payri F, Broatch A, Serrano JR, Piqueras P. Experimental-theoretical methodology for determination of inertial pressure drop distribution and pore structure properties in wall-flow diesel particulate filters (DPFs). Energy 2011;36:6731–44.

[41] Serrano JR, Arnau FJ, Piqueras P, García-Afonso O. Packed bed of spherical particles approach for pressure drop prediction in wall-flow DPFs (diesel particulate filters) under soot loading conditions. Energy 2013;58:644–54.

[42] Serrano JR, Climent H, Piqueras P, Angiolini E. Analysis of fluid-dynamic guidelines in diesel particulate filter sizing for fuel consumption reduction in post-turbo and pre-turbo placement. Appl Energ 2014;132:507–23.

## Nomenclature

| | |
|---|---|
| 0D | Zero-dimensional |
| 1D | One-dimensional |
| DOC | Diesel oxidation catalyst |
| DPF | Diesel particulate filter |
| ECU | Electronic control unit |
| EGR | Exhaust gas recirculation |
| EUDC | Extra urban driving cycle |
| FSCR | Filter and selective catalytic reduction |
| HD | Heavy-duty |
| LNT | Lean $NO_x$ trap |
| NEDC | New European Driving Cycle |
| RDE | Real Driving Emissions |
| SCR | Selective catalytic reduction |
| UDC | Urban driving cycle |
| VGT | Variable geometry turbine |
| WLTP | World-Harmonized Light-Duty Vehicles Test Procedure |

## List of Tables



## List of Figures

- Figure 10.- Comparison between filtrated and weighed soot mass in the DPF after the test during 25 consecutive NEDCs as a function of the aftertreatment system configuration.
- Figure 11.-Load transient test under cold wall operation from motoring conditions to 80% in engine load at 2000 rpm: engine performance as a function of the aftertreatment configuration.
- Figure 12.- Load transient test under cold wall operation from motoring conditions to 80% in engine load at 2000 rpm: boosting conditions as a function of the aftertreatment configuration.
- Figure 13.- Load transient test under cold wall operation from motoring conditions to 80% in engine load at 2000 rpm: gas temperature in different locations of the exhaust line as a function of the aftertreatment configuration.
- Figure 14.- Scheme of the pre-turbo aftertreatment configuration with two stage boosting architecture based on mechanical assistance.
- Figure 15.- Engine scheme in OpenWAM's interface with pre-turbo DPF&DOC configuration.
- Figure 16.- Load transient test under cold wall operation from motoring conditions to 80% in engine load at 2000 rpm: modelling of the engine performance as a function of the aftertreatment configuration and the turbocharging architecture.
- Figure 17.- Load transient test under cold wall operation from motoring conditions to 80% in engine load at 2000 rpm: modelling of the variation in bsfc as a function of the aftertreatment configuration and the turbocharging architecture.
- Figure 18.- Load transient test under cold wall operation from motoring conditions to 80% in engine load at 2000 rpm: modelling of the exhaust line thermal conditions as a function of the aftertreatment configuration and the turbocharging architecture.
- Figure 19.- Load transient test under hot wall operation from motoring conditions to 80% in engine load at 2000 rpm: engine performance as a function of the aftertreatment configuration.
- Figure 20.- Load transient test under hot wall operation from motoring conditions to 80% in engine load at 2000 rpm: boosting conditions as a function of the aftertreatment configuration.

Table 1: Main characteristics of the engine.

| | |
|---|---|
| Type | HSDI Diesel passenger car engine |
| Displacement | 1997 $cm^3$ |
| Bore | 85 mm |
| Stroke | 88 mm |
| Number of cylinders | 4 in line |
| Number of valves | 4 per cylinder |
| Compression ratio | 18:1 |
| Maximum power @ speed | 100 kW @ 4000 rpm |
| Maximum torque @ speed | 320 Nm @ 1750 rpm |

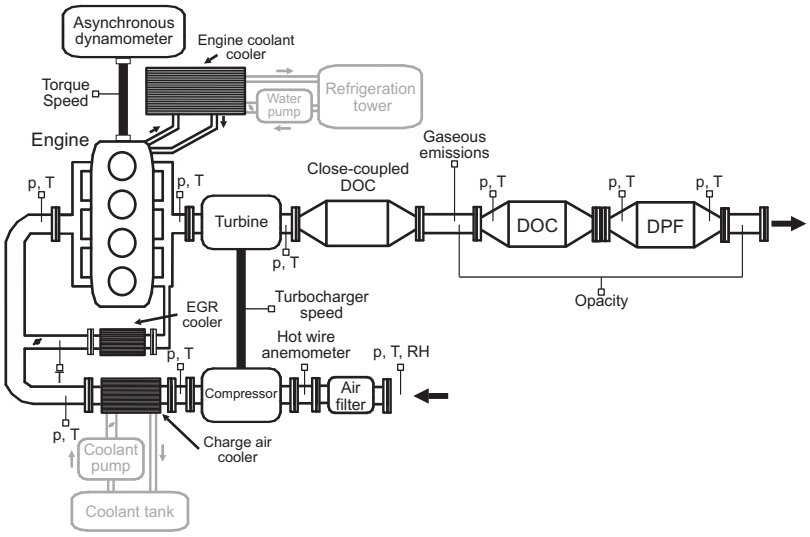


Figure 1: Scheme of the experimental setup and instrumentation with post-turbo aftertreatment placement.

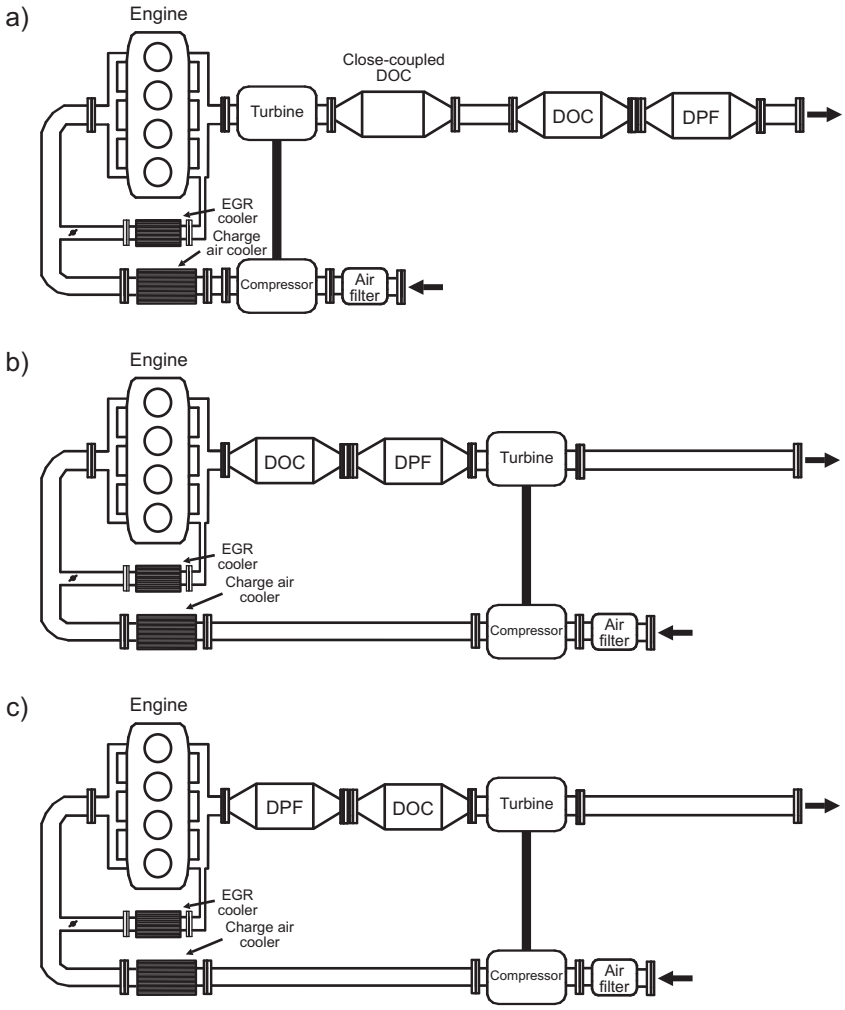


Figure 2: Schemes of the tested exhaust line architectures.

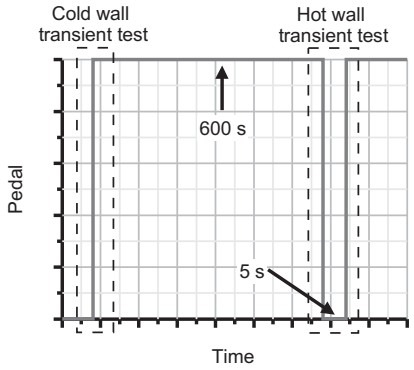


Figure 3: Phases of the load transient tests at constant engine speed.

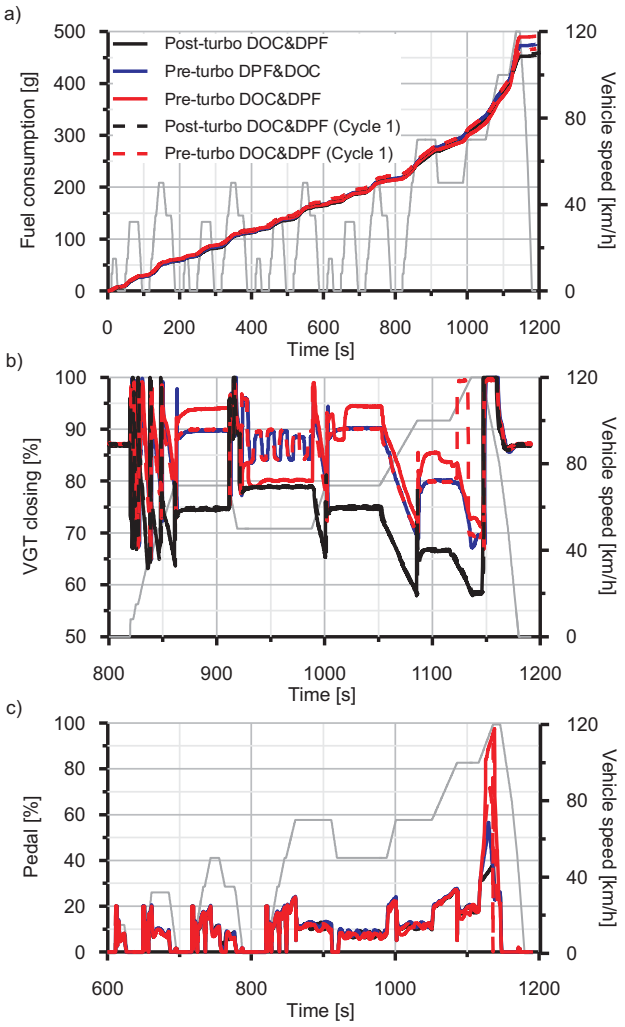


Figure 4: Engine response during the NEDC as a function of the aftertreatment system configuration.

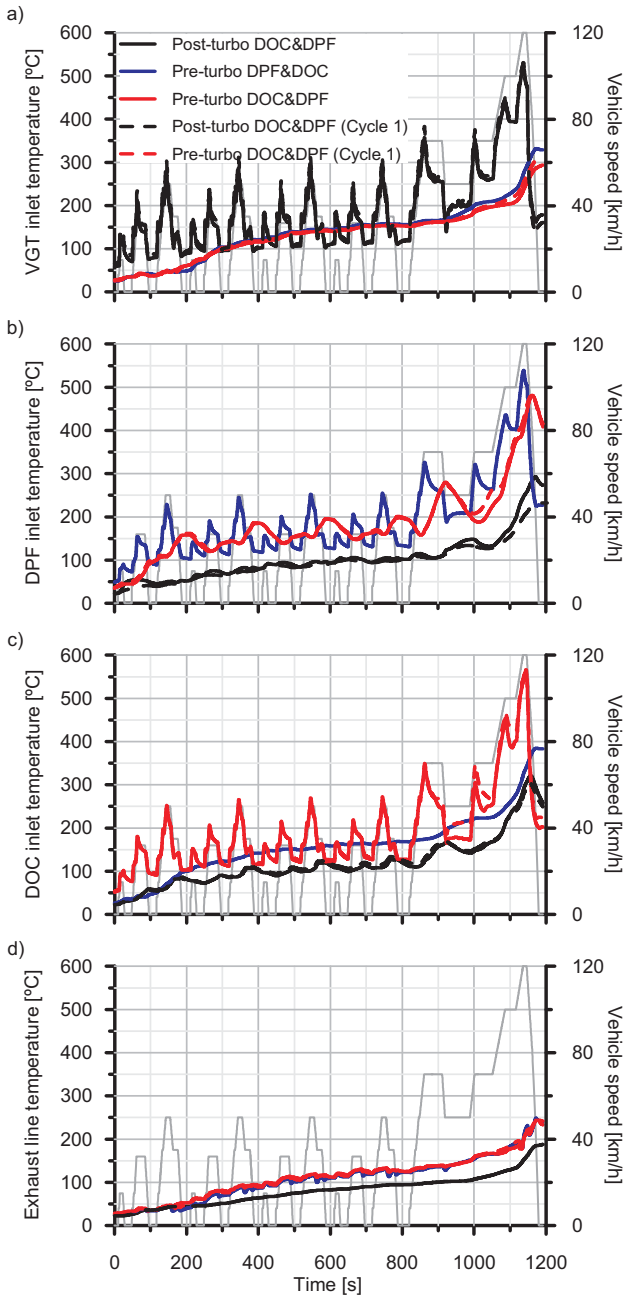


Figure 5: Temperature profile along the engine exhaust line during the NEDC as a function of the aftertreatment system configuration.

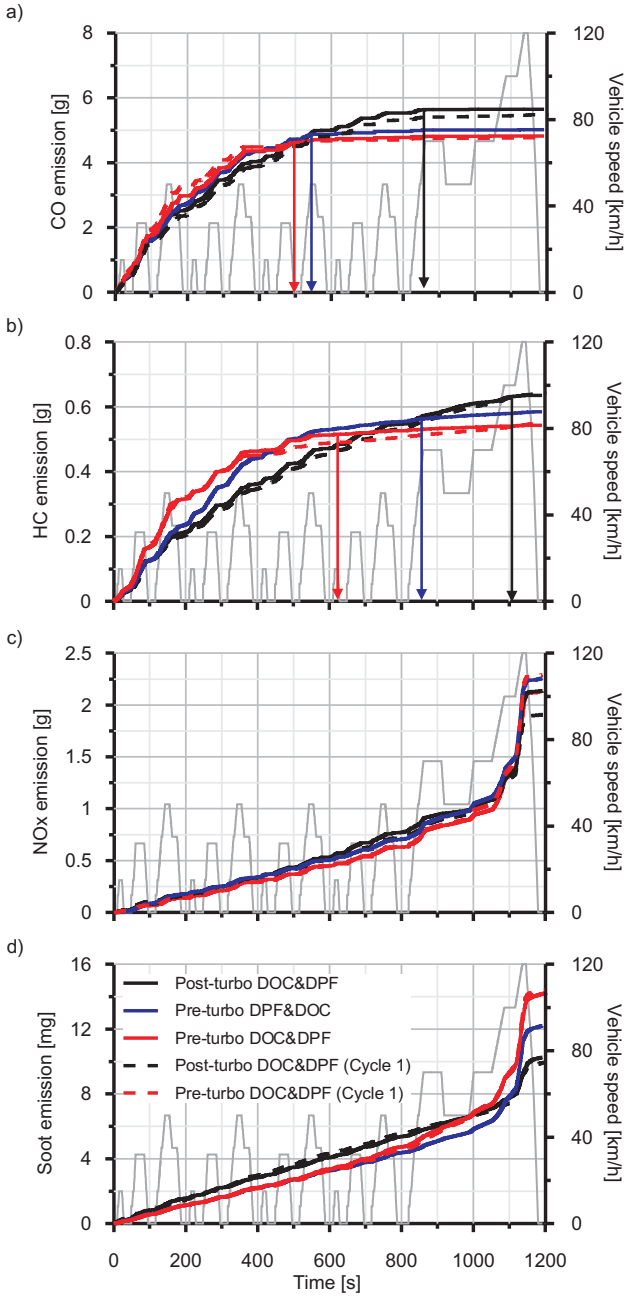


Figure 6: Evolution of regulated tailpipe emissions during the NEDC as a function of the aftertreatment system configuration.

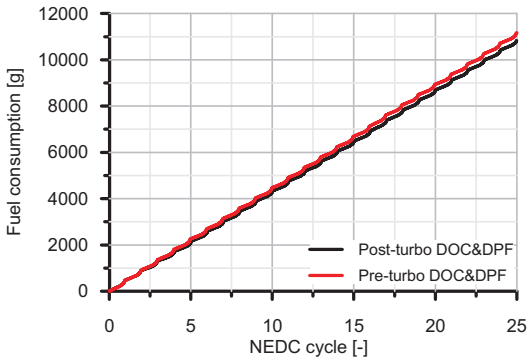


Figure 7: Accumulated fuel consumption during the 25 consecutive NEDCs test as a function of the aftertreatment system configuration.

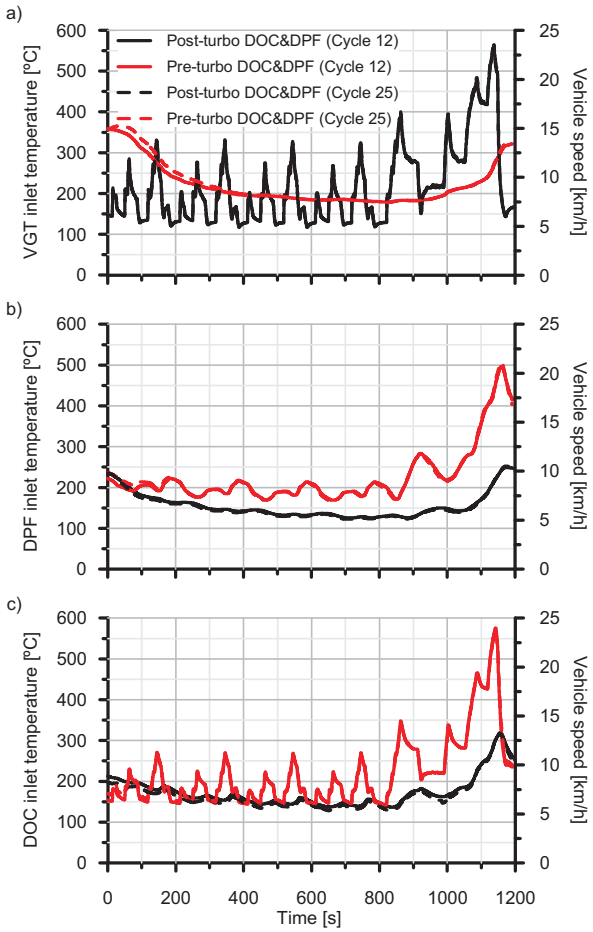


Figure 8: Temperature profile along the engine exhaust line during hot NEDCs as a function of the aftertreatment system configuration.

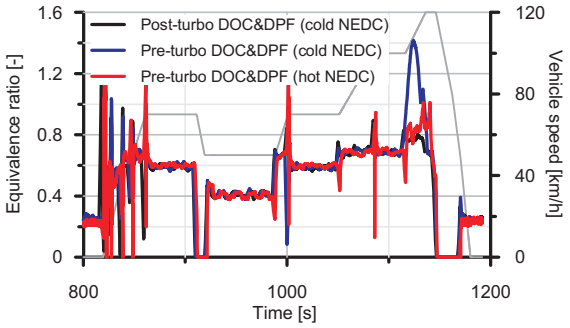


Figure 9: Equivalence ratio during the EUDC phase of cold and hot NEDCs with pre-turbo DOC&DPF configuration.

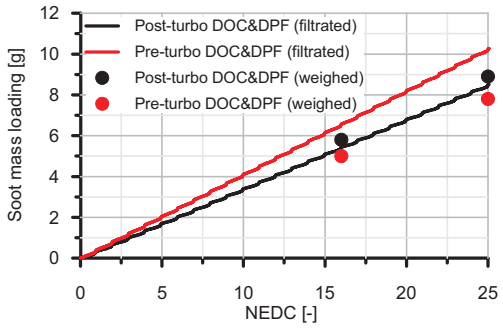


Figure 10: Comparison between filtrated and weighed soot mass in the DPF after the test during 25 consecutive NEDCs as a function of the aftertreatment system configuration.

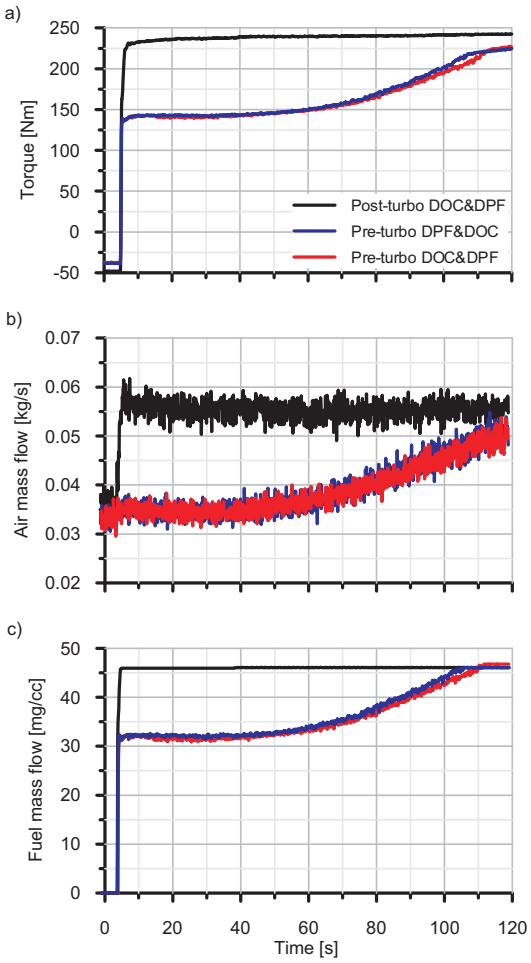


Figure 11: Load transient test under cold wall operation from motoring conditions to 80% in engine load at 2000 rpm: engine performance as a function of the aftertreatment configuration.

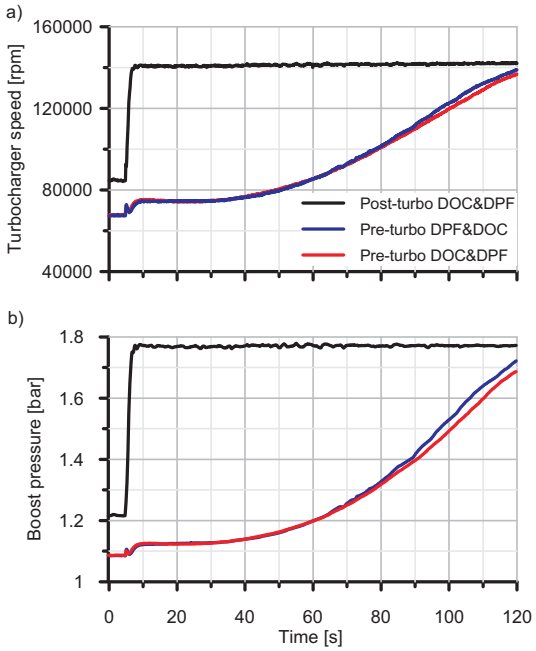


Figure 12: Load transient test under cold wall operation from motoring conditions to 80% in engine load at 2000 rpm: boosting conditions as a function of the aftertreatment configuration.

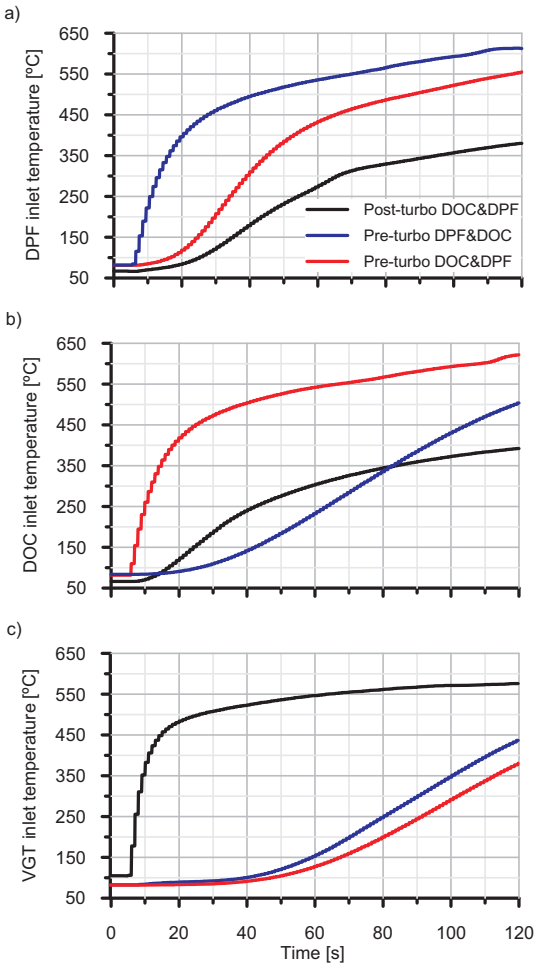


Figure 13: Load transient test under cold wall operation from motoring conditions to 80% in engine load at 2000 rpm: gas temperature in different locations of the exhaust line as a function of the aftertreatment configuration.

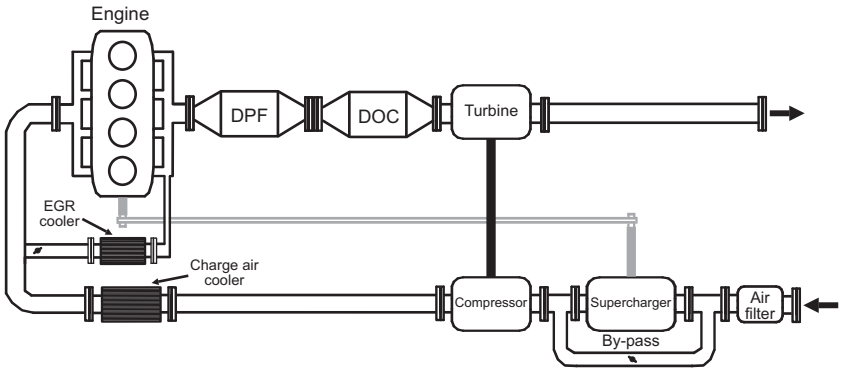


Figure 14: Pre-turbo aftertreatment configuration with two stage boosting architecture based on mechanical assistance.

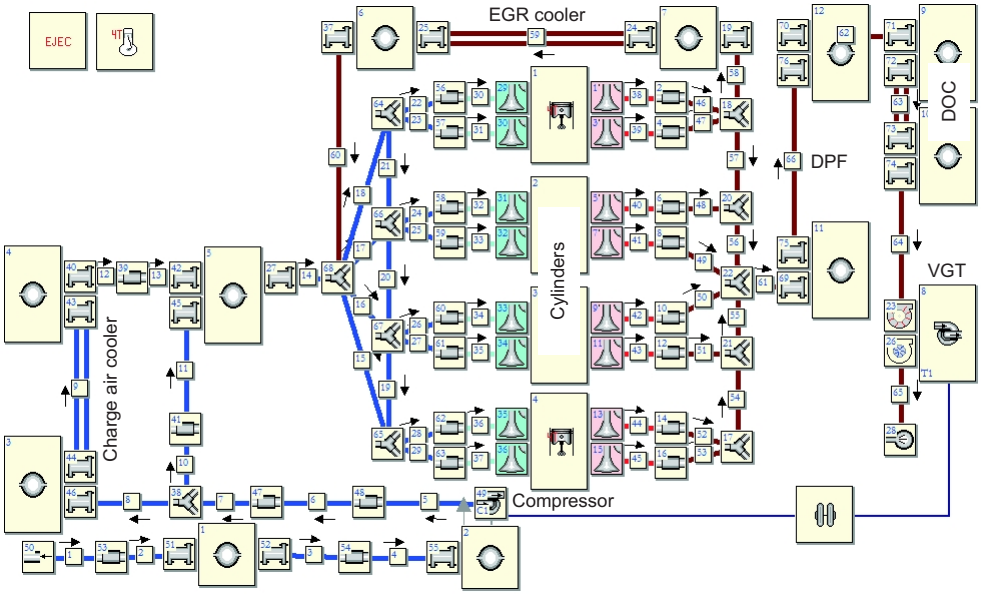


Figure 15: Engine scheme in OpenWAM's interface with pre-turbo DPF&DOC configuration.

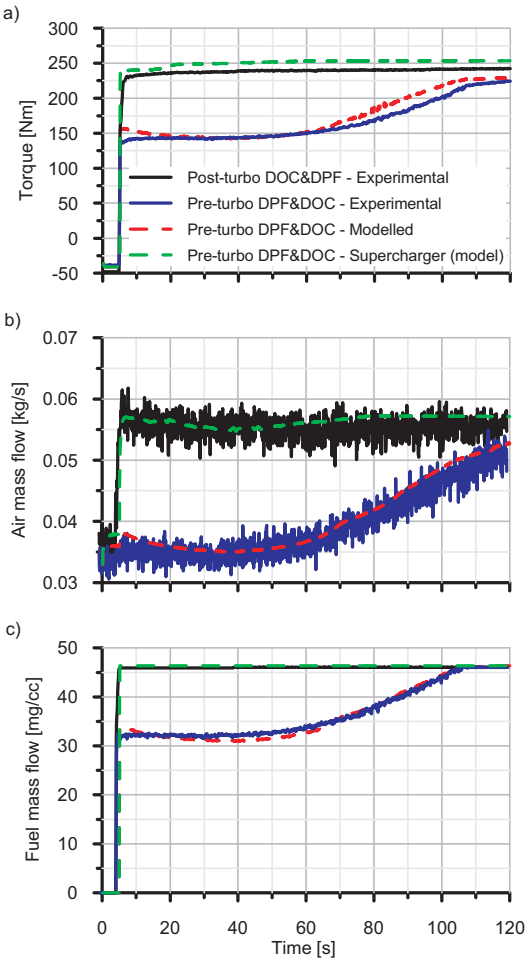


Figure 16: Load transient test under cold wall operation from motoring conditions to 80% in engine load at 2000 rpm: modelling of the engine performance as a function of the aftertreatment configuration and the turbocharging architecture.

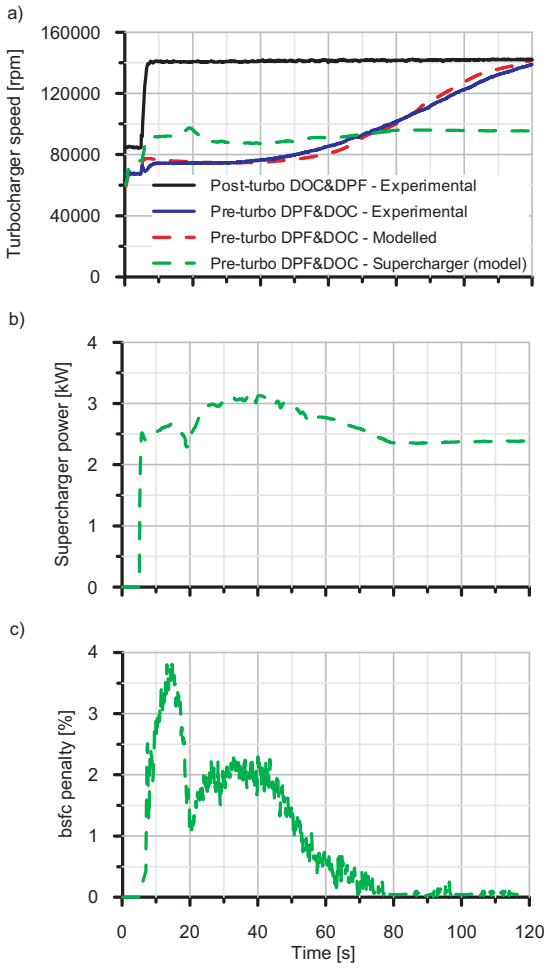


Figure 17: Load transient test under cold wall operation from motoring conditions to 80% in engine load at 2000 rpm: modelling of the variation in bsfc as a function of the aftertreatment configuration and the turbocharging architecture.

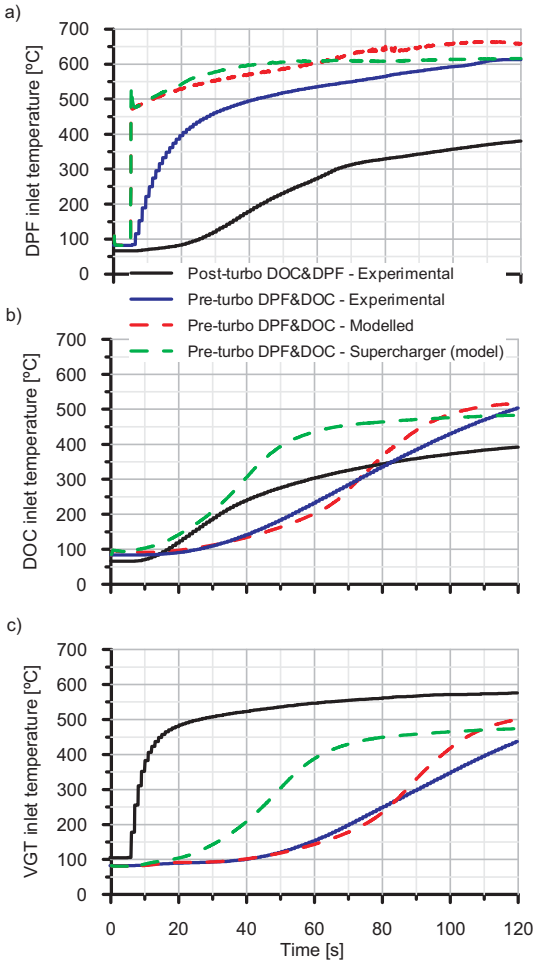


Figure 18: Load transient test under cold wall operation from motoring conditions to 80% in engine load at 2000 rpm: modelling of the exhaust line thermal conditions as a function of the aftertreatment configuration and the turbocharging architecture.

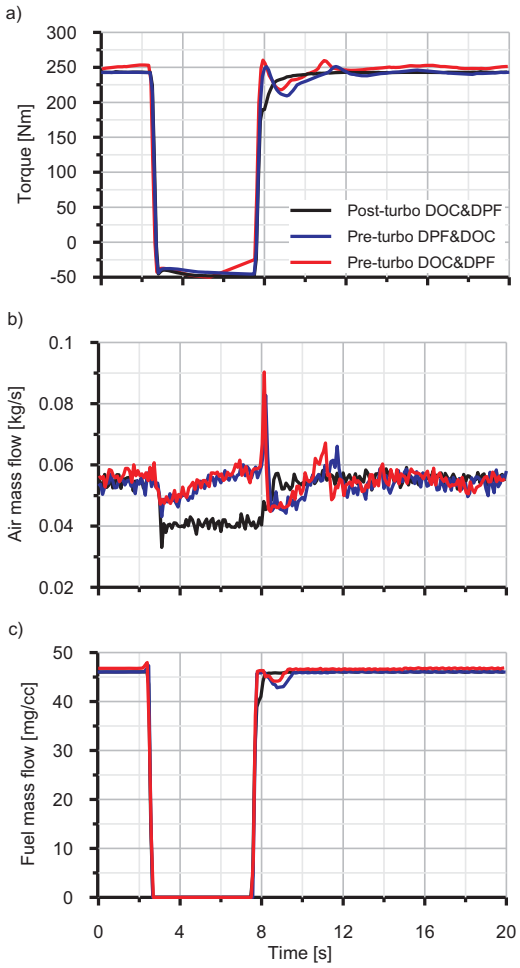


Figure 19: Load transient test under hot wall operation from motoring conditions to 80% in engine load at 2000 rpm: engine performance as a function of the aftertreatment configuration.

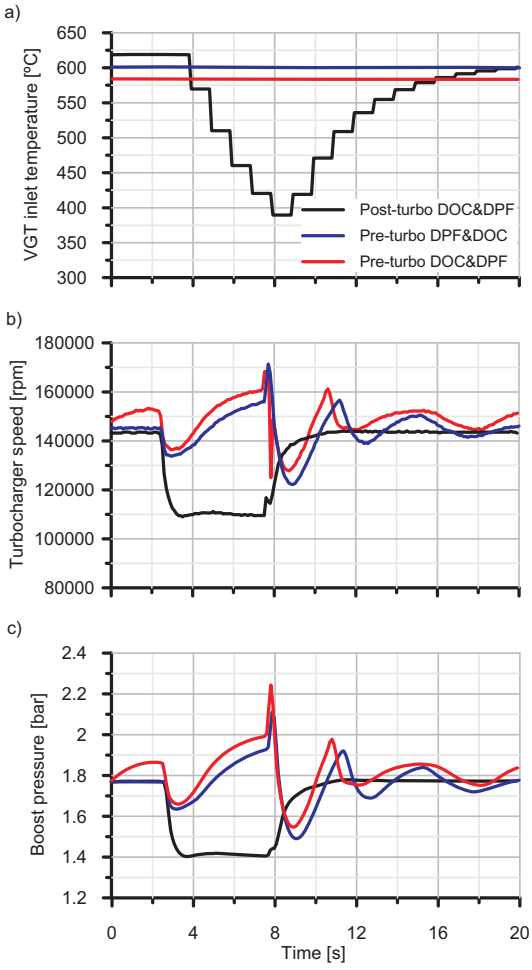


Figure 20: Load transient test under hot wall operation from motoring conditions to 80% in engine load at 2000 rpm: boosting conditions as a function of the aftertreatment configuration.